Plasmonic Nanophotonics and its applications

K. R. Chen*, J. S. Hong** and A. V. Goncharenko***

* Department of Physics, National Cheng Kung University
1 University Road, Tainan 70101, Taiwan, ROC
Research Center for Energy Technology and Strategy, National Cheng Kung University
1 University Road, Tainan 70101, Taiwan, ROC, chenkr@mail.ncku.edu.tw
** Department of Photonics, National Cheng Kung University
1 University Road, Tainan 70101, Taiwan, ROC, l7897117@mail.ncku.edu.tw
*** Institute of Semiconductor Physics, National Academy of Sciences of Ukraine
Kyiv 03028, Ukraine
Department of Physics, National Cheng Kung University
1 University Road, Tainan 70101, Taiwan, ROC, a_v_goncharenko@yahoo.com

ABSTRACT

The EM waves and surface plasmnon polaritons can be controlled by the metallic nanostructures and surrounded medium. We discuss methods for the manipulation, and demonstrate some examples of our reasearch achievements .

Keywords: plasmoics, nanophotonics, subwavelength, metamaterial, diffraction limit

1 INTRODUCTION

Study of surface plasmnon polariton (SPP) effect is a fundamental scientific cross-disciplinary research area with academic importance and critical application potential; especially after the discovery of the extraordinary optical transmission (EOT) phenomenon through a subwavelength metallic hole array [1]. SPP is the coupled mode of an electromagnetic wave and free charges on a metal surface. The excitations of the SPPs and surface-plasmon-like modes can be controlled by the metallic nanostructures and surrounded medium. We discuss methods for the manipulation of light and plasmonic properties with nanostructures. To be specific, the generation of a focused or collimated beam that can be beyond the conventional diffraction limit as well as the enhanced transmission in a narrow or broad band can be achieved by innovation subwavelength structures.

2 BEYOND THE DIFFRACTION LIMIT

As a fundamental scientific limitation, diffraction is a general wave phenomenon occurs whenever a traveling wave front encounters and propagates past an obstruction, was first referenced in the work of Leonardo da Vinci in the 1400s and has being accurately described since Francesco Grimaldi in the 1600s [2]. Explanation based on a wave theory was not available until the 1800s.

The diffraction limit restricts the minimum value of the product of the angular divergence and the width of a light beam. For a single aperture, the limitation can be given as $\alpha\lambda$/NA, where λ is the wavelength in vacuum, NA = $n\sin\theta$ is the numerical aperture, n is the refractive index of the medium where the focused light locates, θ is the convergence angle of the light, and the constant α is 0.38, 0.5, and 0.61 for a ring, line, and circular aperture, respectively [2]. Thus, there are two important issues; namely, focusing and collimation.

The excitations of the surface plasmon [3-5] on metallic surfaces and surface-plasmon-like modes [6, 7] are claimed to enhance [1, 8] the transmission of light and to beam/focus [9-11] it through subwavelength holes/slits [12]. The wave function across the slit is close to a constant and drops sharply on the surface. With a plasmonic structure, the wave function inside the structure is generated with the excitation of SPPs and squeezed with the asymmetry. This kind of function bounded within a sublimit scale is not considered in the conventional theories and is not within their scope. As a result, the trasnsmitted light can be manipulated by means of tuning the material optical properties and its geometrical dimension.

Taking the advantage of it, here we demonstrate the innovative approadch of the focusing and collimating of trasmitted light with use of plasmonic effect.

2.1 Plasmonic Focusing Lens

The plasmonics focusing lens beyond the conventional diffraction-limited linewidth (FAB) of half the wavelength [13] are demonstrated in Fig. 1(a), including a metallic film with a double slit and a patterned exit structure.

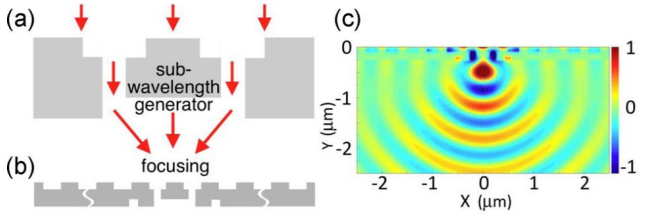

Fig. 1 (a) Schematic diagram of the structure, and the paths of the light transmitted, bent, and focused. (b) Schematic lens made of a silver film. (c) FDTD snapshot of the H_z

field at $t = t_f + 0.12$, where t_f is defined when H_z at the focus spot arises to maximum [14].

A structured thin silver film with 20 and 2 grooves at the incident and exit side, respectively, is employed as our FAB lens, as shown in Fig. 1(b), where the depth, width, and distance in between the periodical grooves at the incident side are 80, 200, and 200 nm, respectively; the slit width is 80 nm; both the width and depth of grooves at the exit side are 80 nm; the distance between the slit and the exit groove is 160 nm; the film thickness is 280 nm; the thickness and the width of the central strip are 200 nm and 320 nm; the central metal width is 320 nm; the exit width is 480 nm, respectively. The refractive index of silver used for $\lambda = 633$ nm is $0.134 + i3.99$.

A finite-difference time-domain (FDTD) simulation is employed to verify. The system has 1600 × 1000 cells of the Yee space lattice with a unit cell size of 5 nm. The top of the silver film is at the $y = 800$ cell, defined as $y = 0$. The time, t, is normalized to the light period, and the time step is 0.005. Fig. 1(c) shows a snapshot of the focused magnetic field. The linewidth of the focus spot can be defined by the FWHM of the field energy. Fig. 2 shows that the FWHM of the time-averaged H_z field energy agrees well with that for the sapshot of the H_z field energies. While the peak intensity of the focused light remains higher than unity, the FWHMs at the normalized distance kr up to 4.17 are smaller than the diffraction limited linewidth of $\lambda/2$. Obviously, the diffraction limit has been locally overcome by a result at the intermediate zone with regard to the focused light [14].

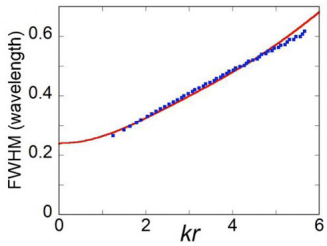

Fig. 2 FWHM versus normalized r profiles of the time-averaged H_z field energy (red solid curve) and the snapshot of the H_z field energy (blue squares), where r is the y distance from the metal surface [14].

For a propagating (near) field [15], the electric field is in phase (out of phase) with the magnetic field so that the Poynting vector (i.e., the energy flow) is not (is) zero. The time-averaged Poynting vector in the original y propagation direction [shown in Fig. 3(a)] also indicates that the focused fields are propagating and hence are capable of traveling to the far zone [15]; this makes the FAB lens superior to evanescent near-field solutions [16, 17] for many critical applications. The involvement of the near field is quantitatively investigated in depth. At the middle location of the central metal strip surface, the Hz field is out of phase with the Ex field and in phase with the surface current $-Jx$, as shown in Fig. 3(b). Thus, it is dominated by the near field. But, at $t = tf + 0.12$, the focused light has moved out. Its surface Hz field is close to zero, on average, and is a small positive number at the middle. The focused Ex field has a similar contour as the Hz field. The ratio and locations of their peaks determine the impedance Z. The estimated propagating Ex field is ZHz, which agrees well with the measured Ex, as shown in Fig. 3(c). This is one more indication [15] for the focusedlight to be dominated by the radiative field, as also evidenced by the propagation of the Ex field at different times [shown in Fig. 3(d)]. At the time 0.01 later, the Hz field at the middle has dropped to a negative value very close to zero. The estimated propagating Ex field along kr based on the analytical theory is in good agreement with the focused field obtained from the simulation. The near-Ex field, including the intermediate field, results from their difference and is decreasing away from the surface as expected with the length of half the field energy being $kr = 0.476$ ($<0.1\lambda$). The effect of the near field is negligible at the intermediate zone of $2 < kr < 4$, where the linewidth of the focused light is smaller than the diffraction-limited value. The result confirms that the near field is negligible in our focusing.

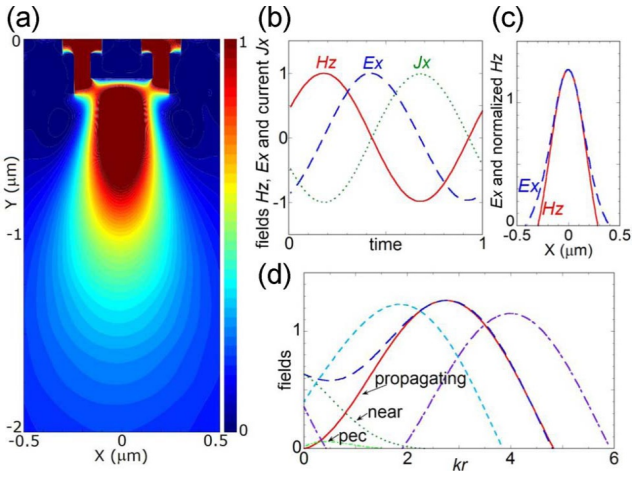

Fig. 3 Poynting vector contours and the field profiles. (a) Time-averaged contours of the Poynting vector (i.e., the energy flow) in the y direction. (b) Temporal profiles of the magnetic field H_z (red solid curve), the electric field E_x (blue dashed curve), and the current J_x (green dotted curve) at $x = 0$ of the central metal surface. (c) x profiles of peak E_x (blue dashed curve) and ZH_z (red solid curve) fields at $t = t_f + 0.12$, where $|Z| = 0.832$ and the phase is three cells or 0.0237λ. (d) r profiles of the E_x field at $t = t_f$ (light blue short dashed curve), $t = t_f + 0.13$ (blue dashed curve), and $t_f + 0.29$ (purple short dashed curve and dashed curve) when the FWHM of the Hz energy is still smaller than $\lambda/2$, as well as the ZH_z field (red solid curve, the estimated propagating E_x field, where $|Z| = 0.840$), the near E_x field (dark green dotted curve, the difference of the overall and propagating fields), and the near-E_x field for the case of an almost perfect electric conductor (light green dotted curve and short dashed curve) [14].

Besides simulation, we also experimentally verify the FAB lens [18]. A similar structure is fabricated by a foucus ion beam, as shown in Fig. 4(a). The double slit, patterned exit structure, and 2 grooves are perforated on a thin silver film on the fused silica substrate, as designed by FDTD simulation. The dimension of each structure is as the same as the aforementioned one. The incident light, with its electric field polarized in the *x* direction, propagates upward through the double slit.

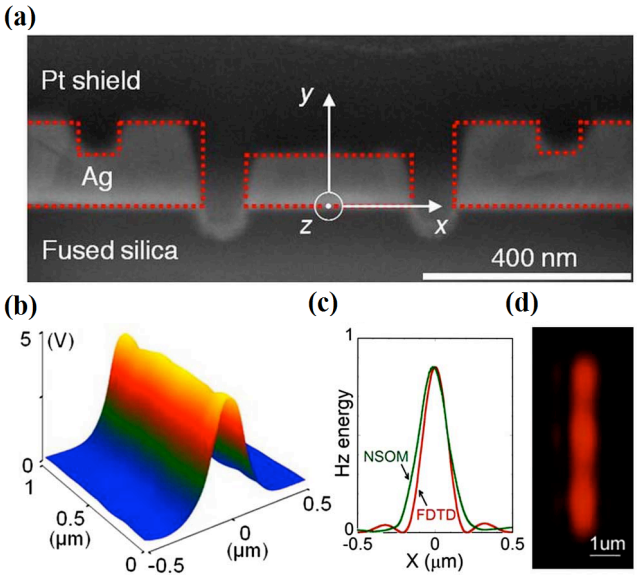

Fig. 4 (a) Views of the lens (slit length, 4 μm) using a silver film on fused silica substrate; the Pt shield was soley added for the purpose of making this cross-sectional view. The red dotted lines define the film structure. (b) *x*–*z* distribution of the NSOM measurement. (c) Profiles of the NSOM measurement and and the focused H_z field energy from the FDTD simulation. (d) Picture taken by the OM [18].

A measurement of the transmitted light by a near-field scanning optical microscopy (NSOM) is shown in Fig. 4(b). The homogenity of the measurement profile along the *z* direction is good enough to evidence the quality of the film and the structure. The FWHM across the slit structure in the *x* direction is obviously smaller than half wavelength and thus, the diffraction limit. The experimental profile averaged over the *z* direction is found to be in a good agreement with the focused light calculated from the FDTD simulation, as shown in Fig. 4(c). Figure 4(d) indicates that the focused light can propagate out and can be measured by the OM located 500λ away from the FAB lens. This confirms that the focused fields have the momentum to propagate to the far zone [15], as is also evidenced by the Poynting vector (not shown).

The physical mechanisms of the innovative approach using a miniature FAB lens are demonstrated. Besides, the light focusing process is expected to open up a wide range of application possibilities (e.g., sensing, photolithography, biological and physical systems, and photonic/plasmonic circuits [19]), especially with regard to the capabilities of the focused light being able to propagate, tuning the focal point position and reducing the sizes of the focused light spot and the corresponding devices.

2.2 Collimated Light Beam

From the aspect of angle divergence of diffraction limit, we simulate and model the generation of super-collimated light beam through a novel metallic nano-structured subwavelength film. The collimated beam is almost without divergence from the simulation. This is a breakthrough on the angular divergence aspect of the diffraction limit.

To verify, both an analytical model for the wave function and experimental measurement of the transmitted light have been preliminarily obtained.

If feasible, the super-collimation provides an opportunity for fabricating high-aspect-ratio holes needed by the through-silicon vias (TSV) to make the 3D circuits.

3 PLASMONIC FILTER

SPPs can resonate with the incident electromagnetic wave of specific wavelength. We propose different plasmonic nanostructures to allow the light of red, green, and blue, respectively, to pass through. This can replace conventional optical filters, which is preliminarily verified by one of the primary semiconductor companies in the world. To increase the transmission efficiency, we also study the cascade/hybridization effect of SPPs.

4 METAMATERIAL WITH DESIRED BROADBAND OPTICAL PROPERTIES

The development of metamaterials that possess desired optical properties over a spectral band is a problem of fundamental importance; its solution could considerably improve the performance of many existing optical devices and allow new devices.

Dealing with nanostructured metal/dielectric composites with a specified spatial configuration, within the framework of the effective medium theory, we obtain an approximation for their effective permittivity. Making use of this approximation, we propose a scheme for designing above metamaterials. As particular examples, we consider quasi one dimensional metamaterials with ultralow refractive index, a high absorption, and those possessing pass-band filtering [20-22].

We consider a layered photonic crystal which consists of unit cells with the local permittivity $\varepsilon(z)$ in both the *x*- and *y*-direction and varying in the *z*-direction and assume that the external electric field is applied along the *z* axis. As an example, in Fig. 5 we sketch a basic geometry which makes up an array of parallel dielectric (metal) pores of varied width in a metal (dielectric) host. As the local permittivity varies along the *x*-axis as well, the composite becomes 2D rather than 1D. However, if the size of the unit cell in the *x*-direction is much smaller, each layer in the long-wavelength approximation may be considered as macroscopically homogeneous, and the composite may be

considered as quasi-1d. Due to the continuity of the electric field which is tangential to the metal/dielectric interfaces, the permittivity of the *i*th layer may be written as

$$\varepsilon_i = f_i\varepsilon_1 + (1 \quad f_i)\varepsilon_2, \tag{1}$$

where ε_1 and ε_2 are the permittivities of the metallic and dielectric phases, respectively, and f_i is the volume fraction of the metal phase in the *i*th layer. In the example, the dielectric constant is expressed with Drude model. If the unit cell is of subwavelength size, the effective permittivity may be simply written as the harmonic average

$$\varepsilon_{eff} = N[\sum_{i=1}^{N} 1/\varepsilon_i]^{-1}. \tag{2}$$

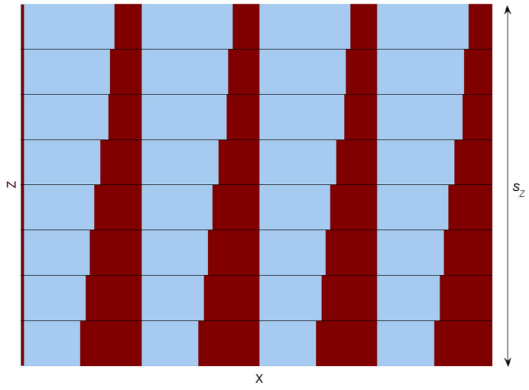

Fig. 5 Four unit cells representing a possible geometry.

Tailoring the metamaterial with desired optical properties in a specific frequency is decided by a specific layer. Thus, Eq. (2) lets us extend from single frequency to a broadband due to the composition of the hybrid layers. Fig. 6 demonstrates the desired optical properties of the metamaterials.

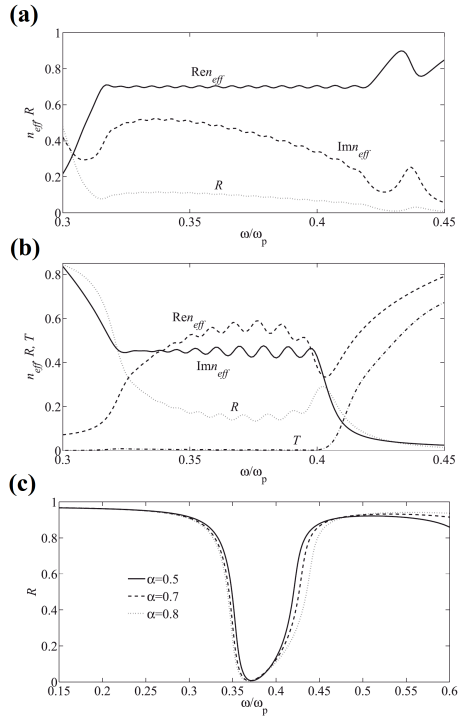

Fig. 6 Desired optical properties of the metamaterial in a band. (a) Ultralow refractive index. (b) High absorption efficiency. (c) Pass-band filtering [21].

5 SUMMARY

We have shown the methods to manipulate light. To demonstrate, the generation of a focused or collimated beam that can be beyond the conventional diffraction limit as well as the enhanced transmission in a narrow or broad band can be achieved by innovation subwavelength structures. We expect this could have wide application potential in nanophotonic devices.

REFERENCES

[1] T. W. Ebbesen, H. J. Lezec, H. F. Ghaemi, T. Thio, and P. A. Wolff, Nature 391, 667 (1998).
[2] M. Born and E. Wolf, Principles of Optics (Pergamon, 2005).
[3] R. H. Ritchie, Phys. Rev. 106, 874 (1957).
[4] J. B. Pendry, Science 285, 1687 (1999).
[5] W. L. Barnes, A. Dereux, and T. W. Ebbesen, Nature 424, 824 (2003).
[6] J. B. Pendry, L. Martin-Moreno, and F. J. Garcia-Vidal, Science 305, 847 (2004).
[7] W. Barnes and R. Sambles, Science 305, 785 (2004).
[8] H. T. Liu and P. Lalanne, Nature 452, 728 (2008).
[9] H. J. Lezec, A. Degiron, E. Devaux, R. A. Linke, L. Martin-Moreno, F. J. Garcia-Vidal, and T. W. Ebbesen, Science 297, 820 (2002).
[10] F. J. Garcia-Vidal, L. Martin-Moreno, H. J. Lezec, and T. W. Ebbesen, Appl. Phys. Lett. 83, 4500 (2003).
[11] L. Markley, A. M. H. Wong, Y. Wang, and G. V. Eleftheriades, Phys. Rev. Lett. 101, 113901 (2008).
[12] H. A. Bethe, Phys. Rev. 66, 163 (1944).
[13] K. R. Chen, Bull. Am. Phys. Soc. 52, 202 (2007).
[14] K. R. Chen, Opt. Lett. 35, 3763 (2010).
[15] J. D. Jackson, Classical Electrodynamics, 3rd ed. (Wiley, 1998).
[16] J. B. Pendry, Phys. Rev. Lett. 85, 3966 (2000).
[17] N. Fang, H. Lee, C. Sun, and X. Zhang, Science 308, 534 (2005).
[18] K. R. Chen, et al., Opt. Lett. 36, 4497 (2011)
[19] T. W. Ebbesen, C. Genet, and S. I. Bozhevolnyi, Phys. Today 61, 44 (2008).
[20] A. V. Goncharenko and K. R. Chen, J. Nanophotonics 4, 041530 (2010).
[21] A. V. Goncharenko, V. U. Nazarov, and K. R. Chen, Appl. Phys. Lett. 101, 071907 (2012).
[22] A. V. Goncharenko, V. U. Nazarov, and K. R. Chen, Opt. Mater. Express 3, 143 (2013).